CHEMISTRY
A EUROPEAN JOURNAL

FULL PAPER

DOI: 10.1002/chem.201201065

Highly Dispersed TiO_6 Units in a Layered Double Hydroxide for Water Splitting

Yufei Zhao,[a] Pengyun Chen,[a] Bingsen Zhang,[b] Dang Sheng Su,[b] Shitong Zhang,[a] Lei Tian,[a] Jun Lu,[a] Zhuoxin Li,[c] Xingzhong Cao,[c] Baoyi Wang,[c] Min Wei,*[a] David G. Evans,[a] and Xue Duan[a]

Abstract: A family of photocatalysts for water splitting into hydrogen was prepared by distributing TiO_6 units in an MTi-layered double hydroxide matrix (M = Ni, Zn, Mg) that displays largely enhanced photocatalytic activity with an H_2-production rate of 31.4 μmol h^{-1} as well as excellent recyclable performance. High-angle annular dark-field scanning transmission electron microscopy (HAADF-STEM) mapping and XPS measurement reveal that a high dispersion of TiO_6 octahedra in the layered doubled hydroxide (LDH) matrix was obtained by the formation of an M^{2+}-O-Ti network, rather different from the aggregation state of TiO_6 in the inorganic layered material $K_2Ti_4O_9$. Both transient absorption and photoluminescence spectra demonstrate that the electron–hole recombination process was significantly depressed in the Ti-containing LDH materials relative to bulk Ti oxide, which is attributed to the abundant surface defects that serve as trapping sites for photogenerated electrons verified by positron annihilation and extended X-ray absorption fine structure (EXAFS) techniques. In addition, a theoretical study on the basis of DFT calculations demonstrates that the electronic structure of the TiO_6 units was modified by the adjacent MO_6 octahedron by means of covalent interactions, with a much decreased bandgap of 2.1 eV, which accounts for its superior water-splitting behavior. Therefore, the dispersion strategy for TiO_6 units within a 2D inorganic matrix can be extended to fabricate other oxide or hydroxide catalysts with greatly enhanced performance in photocatalysis and energy conversion.

Keywords: double hydroxides · layered compounds · photochemistry · titanium · water splitting

Introduction

The search for suitable semiconductors as photocatalysts for the splitting of water into hydrogen by using solar energy is one of the primary missions of material science, which has received considerable attention on account of the increasing number of global energy crises.[1] Since the discovery of the first water-splitting system based on TiO_2, various inorganic materials have been developed as catalysts for this reaction.[2] Among them, layered structure compounds that contain Ti^{4+}, Nb^{5+}, or Ta^{5+} with a negatively charged plane provide spatially separate reduction and oxidation reaction sites located in their interlayer region and thus exhibit much higher activity for water splitting than the "bulk-type" catalysts such as TiO_2.[3,4] $K_2Ti_4O_9$, as a member of a series of layered materials $M_2O{\cdot}nTiO_2$ (M = Na, K, Rb, Cs, Tl; n = 0.5, 1.0, or 2.0),[5] consists of edge- and corner-shared TiO_6 octahedra separated by a K^+ layer, which has been widely used as a photocatalyst for the decomposition of pollutants as well as water splitting into hydrogen.[6] However, the major obstacle for this system is that the catalyst displays low energy-conversion efficiency as a result of inefficient photochemical charge separation, which is caused by the aggregation of TiO_6 units.[7] Recent theoretical and experimental studies have demonstrated that a highly dispersed network of transitional cations would certainly increase the mobility of electron holes and contribute significantly to the enhancement of catalytic activity.[8a–c] Frei and Hashimoto et al. demonstrated the use of metal-to-metal charge transfer (MMCT) of heterobimetallic assemblies as a new class of silicate sieve photocatalysts.[8] Therefore, to meet the requirements of high-performance catalysts, the development of new materials or methodologies for obtaining photocatalytic H_2 production catalysts with highly dispersed active sites remains a significant goal.[9a–c] This motivated us to

---

[a] Y. Zhao, P. Chen, S. Zhang, L. Tian, Prof. J. Lu, Prof. M. Wei, Prof. D. G. Evans, Prof. X. Duan
State Key Laboratory of Chemical Resource Engineering
Beijing University of Chemical Technology
100029, Beijing (P.R. China)
Fax: (+86) 10-64425385
E-mail: weimin@mail.buct.edu.cn

[b] Dr. B. Zhang, Prof. D. S. Su
Shenyang National Laboratory of Materials Science
Institute of Metal Research
Chinese Academy of Sciences
Shenyang 110016 (P.R. China)

[c] Dr. Z. Li, Prof. X. Cao, Prof. B. Wang
Institute of High Energy Physics
Chinese Academy of Sciences
Beijing 100049 (P.R. China)

Supporting information for this article is available on the WWW under http://dx.doi.org/10.1002/chem.201201065.

© 2012 Wiley-VCH Verlag GmbH & Co. KGaA, Weinheim

take up the challenge of distributing TiO_6 units within an inorganic matrix with high dispersion, so as to enhance the efficiency of charge separation and improve its water-splitting performance.

Among 2D inorganic matrices (e.g., smectite clays, metal phosphates, phosphonates, layered metal oxides, as well as graphene),[9d–f] layered double hydroxides (LDHs) are important layered clays that are generally expressed by the formula $[M^{2+}_{1-x}M^{3+}_{x}(OH)_2]^{x+}(A^{n-})_{x/n}\cdot mH_2O$, in which M^{2+} and M^{3+} are di- and trivalent metal cations and A^{n-} is the anion that compensates for the positive charge of the hydroxide layers.[10] The host structure is based on brucite-like ($Mg(OH)_2$) layers of edge-sharing MO_6 octahedra. On the basis of their specific structure and versatility in chemical composition, LDH materials have been widely used as catalysts and supports, adsorbents for environmental remediation, as well as carriers for biological materials.[10] Recently, García et al. reported doped semiconductors based on three kinds of Zn-containing LDHs that show photocatalytic oxygen-generation activity.[11a] Our group studied a family of visible-light-responsive MCr–LDH (M = Cu, Ni, Zn) materials that exhibit remarkable photocatalytic activity for the decomposition of organic pollutants in water.[11d] Although the semiconductor properties of LDH materials have been reported previously (both for oxygen production and photodecomposition),[11] to the best of our knowledge, their performance for splitting water into hydrogen has not been explored. The layered structure of LDH materials possesses semiconductor properties and facilitates the transfer of the photogenerated electrons to the surface of photocatalysts,[5] which might provide great potential for their application in water splitting. With the assistance of multinuclear NMR spectroscopy, Grey et al. were able to report that the M^{2+} and M^{3+} metal octahedra are distributed in a honeycomb arrangement in LDH layers.[10a] This inspired us to disperse TiO_6 octahedra by other metal octahedra by means of the formation of LDH materials, which would promote the efficiency of electron–hole separation and improve the activity of splitting water into hydrogen.

In this work, MTi–LDHs (M = Ni, Zn, Mg) have been synthesized by a simple coprecipitation method, which exhibit excellent photocatalytic activity for water splitting into hydrogen, 18 times higher than layered $K_2Ti_4O_9$. The intrinsic nature of TiO_6 in the LDH material was explored by high-angle annular dark-field scanning transmission electron microscopy (HAADF-STEM) mapping and XPS measurements, and the results show that the TiO_6 units are highly dispersed in the LDH host layer by the network of M^{2+}-O-Ti, and the metal octahedra are bonded to each other through the metal oxo bridging. Both the transient absorption and photoluminescence spectra measurements indicate a more effective electron–hole separation for the LDH materials than $K_2Ti_4O_9$; this high charge separation is attributed to the higher intensity of surface defects that serve as trapping sites for electrons, which was confirmed by positron annihilation and extended X-ray absorption fine structure (EXAFS). Periodic density functional theoretical calculations demonstrated that the bandgap of the Ti-containing LDHs is ascribed to the transition of TiO_6 octahedra with a gap of 2.1 eV. In addition, these LDH materials can serve as stable, effective, and recyclable photocatalysts for water splitting. Therefore, this work demonstrates a facile strategy for distributing TiO_6 octahedra with high dispersion within a 2D inorganic matrix, which can be potentially applied in the fields of water splitting and solar-energy conversion.

Experimental Section

Materials: Chemical reagents including $Ni(NO_3)_2\cdot 3H_2O$, $Mg(NO_3)_2\cdot 6H_2O$, $Al(NO_3)_2\cdot 9H_2O$, $Zn(NO_3)_2\cdot 6H_2O$, K_2CO_3, NaOH, urea, Na_2CO_3, $NaNO_3$, and HCl were obtained from Beijing Chemical Co., Ltd. α-$Ni(OH)_2$, TiO_2, and $TiCl_4$ were purchased from Sigma–Aldrich Co. Deionized and decarbonated water were used in all experimental processes.

Synthesis of MTi–LDHs (M = Ni, Zn, MgAl): MTi–LDHs (M = Ni, Zn, MgAl) catalysts were prepared by using the coprecipitation method. The synthesis of NiTi–LDHs was similar to that described by He et al.[12] In brief, a $TiCl_4$ solution (0.5 mL; the solution was prepared from $TiCl_4$ and HCl with a volume ratio of 1:1, in which $TiCl_4$ is 0.002 mol), $Ni(NO_3)_2$ (0.008 mol), and urea (0.1 mol) were dissolved in deionized water (100 mL) under vigorous stirring for 27 h at reflux temperature (90 °C). The resulting solid was filtered, washed with deionized water and anhydrous ethanol, and dried at 60 °C. The NiTi–LDHs with different molar ratios of Ni^{2+}/Ti^{4+} were prepared by using the same procedure but by varying the Ni^{2+} dosage.

ZnTi–LDH was prepared by the coprecipitation of zinc and titanium salts from a homogeneous solution according to the literature.[13] $TiCl_4$ (0.22 mL), $Zn(NO_3)_2\cdot 6H_2O$ (1.19 g) and urea (3.0 g) were dissolved in deionized water (100 mL) under vigorous stirring. The resulting reactant was aged in an autoclave at 130 °C for 48 h. The precipitate was centrifuged, washed thoroughly with water, and finally dried at 60 °C for 24 h.

MgAlTi–LDH was prepared by the coprecipitation method with low supersaturation.[14] A solution that contained $Mg(NO_3)_2\cdot 6H_2O$, $Al(NO_3)_3\cdot 9H_2O$, and $TiCl_4$, and another solution that contained NaOH (2.0 M) and Na_2CO_3 (0.50 M) were simultaneously added to a solution of Na_2CO_3 solution (100 mL, 0.01 M), and the pH of the resulting slurry was maintained at approximately 10. The mixture was held at 70 °C for 27 h. The final precipitate was filtered, washed thoroughly with deionized water, and dried at 60 °C for 24 h.

For comparison, the layer structure $K_2Ti_4O_9$ was synthesized according to a solid-state reaction by heating the mixture of TiO_2 and K_2CO_3 (with a 10 % stoichiometric excess amount) at 960 °C for 10 h.[6,15]

Photocatalytic reaction of splitting water into hydrogen: The photocatalytic reaction was carried out using a Splitting water system CEL-SPH2N (Beijing AuLight Co., Ltd.); the setup is shown in Figure S1 in the Supporting Information. The photocatalytic reaction was performed in a Pyrex glass cell with a stationary temperature at 50 °C, which was connected with a closed gas circulation system. LDH material (0.10 g) was suspended in an aqueous solution (150 mL) that contained lactic acid (LA; 0.20 mL) as a sacrificial agent. Pt (0.1 wt %) was loaded onto the surface of LDH in situ by the photoreduction method using H_2PtCl_6 aqueous solution. The suspension was then thoroughly degassed and irradiated using an Xe lamp (300 W). The amount of H_2 produced was analyzed at given time intervals using an online gas chromatograph (GC-7890II; Techcomp. Co., Ltd). The activity of different catalysts was determined on the basis of the average rate of H_2 evolution in the first 5 h.

Characterization: Powder X-ray diffraction (XRD) patterns of the samples were collected using a Shimadzu XRD-6000 diffractometer using a $Cu_{K\alpha}$ source, with a scan step of 0.02° and a scan range between 7 and 70°. Fourier transform infrared spectra were recorded using a Vector22 (Bruker) spectrophotometer in the range 4000–400 cm^{-1} with 2 cm^{-1} of resolution. The standard KBr disk method (1 mg of sample in 100 mg of KBr) was used. UV/Vis spectra were recorded using a Beijing PGENERAL TU-1901 spectrometer in the 350–800 nm wavelength range. Laser flash photolysis experiments were carried out using an Edinburgh LP920 spectrophotometer (Edinburgh Instruments) to record the transient absorption spectra. Sample was excited by using 355 nm output with pulse energies of 1.5 mJ per pulse from an OPO pumped by an Nd:YAG laser (10 Hz, 8 ns) (Continuum Surelite). Data were analyzed by using the online software of the LP920 spectrophotometer. The fitting quality was judged by weighted residuals and a reduced χ^2 value. Fluorescence emission spectra were recorded using an RF-5301PC fluorophotometer (1.5 nm resolution) in the range of 430–500 nm with the excitation wavelength of 366 nm and slit widths of 3 nm. The morphology of the film samples was investigated using a Zeiss Supra 55 scanning electron microscope (SEM) with an accelerating voltage of 20 kV. The morphology of the layered double hydroxide (LDH) flake was characterized by using a JEOL JEM-2010 high-resolution transmission electron microscope with an accelerating voltage of 200 kV. HAADF-STEM measurements were obtained using a Titan 80–300 at 80 kV and an FEI Tecnal G2 F20 U-TWIN instrument at an operating voltage of 200 kV. The specific surface area determination was performed by Brunaer–Emmett–Teller (BET) methods using a Quantachrome Autosorb-1C-VP analyzer. Analyzer X-ray photoelectron spectra (XPS) were recorded using a PHIQ2000 X-ray photoelectron spectrometer equipped with a monochromatized $Al_{K\alpha}$ X-ray source. Positron annihilation experiments were carried out using a fast/slow coincidence ORTEC system with a time resolution of 187 ps full width at half-maximum. A 5×10^5 Bq source of ^{22}Na was sandwiched between two identical samples. The Ni K-edge X-ray absorption near-edge structure (XANES) measurements of the samples were performed at the beam line 1W1B of the Beijing Synchrotron Radiation Facility (BSRF), Institute of High Energy Physics (IHEP), Chinese Academy of Sciences (CAS) at room temperature in the transmission mode.

See the Supporting Information for details on the density functional calculations.

Results and Discussion

Structure and morphology of the Ti-containing LDHs: The MTi–LDHs (M = Ni, Zn, MgAl) were successfully prepared by using a coprecipitation method, the XRD patterns of which are shown in Figure 1. In each case, the reflections exhibit long-range stacking order, which can be indexed to a hexagonal lattice with $R3m$ rhombohedral symmetry, commonly used for the description of LDH structures.[11b,16] In the case of NiTi–LDH, its XRD pattern shows the reflections of (003), (006), (009), and (110) with a basal spacing of 0.722 nm ($2\theta = 12.24°$). The ZnTi– and MgAlTi–LDH show similar reflections with a basal spacing of 0.660 and 0.774 nm, respectively, which is indicative of different interlayer anions. It should be noted that several weak reflections at $2\theta = 22$, 31, and 36° for ZnTi–LDH were observed, which can be assigned to a small amount of zinc hydroxide impurity (PDF card no. 20-1437). The interlayer anions were further confirmed by FTIR spectroscopy (Figure S2 in the Supporting Information). For NiTi–LDH (Figure S2, curve a in the Supporting Information), bands at 2235 and 641 cm^{-1} are assigned to C–N stretching of cyanate anion (CNO^-) and metal–NCO complex, respectively, which results from the incomplete decomposition of urea;[12,16c] an intense absorption band at 1382 cm^{-1} is due to the ν3 (asymmetric stretching) mode of the interlayer CO_3^{2-} anion.[16] This indicates the coexistence of the CNO^- and CO_3^{2-} anions in the NiTi–LDH gallery. In the case of ZnTi–LDH and MgAlTi–LDH (Figure S2, curves b and c in the Supporting Information), bands at 1659 and 1387 cm^{-1} demonstrate the presence of carbonate (CO_3^{2-}).

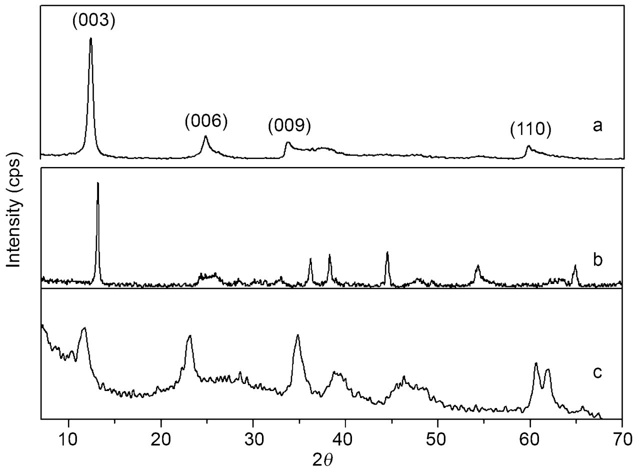

Figure 1. XRD patterns of a) NiTi–LDH, b) ZnTi–LDH, and c) MgAlTi–LDH.

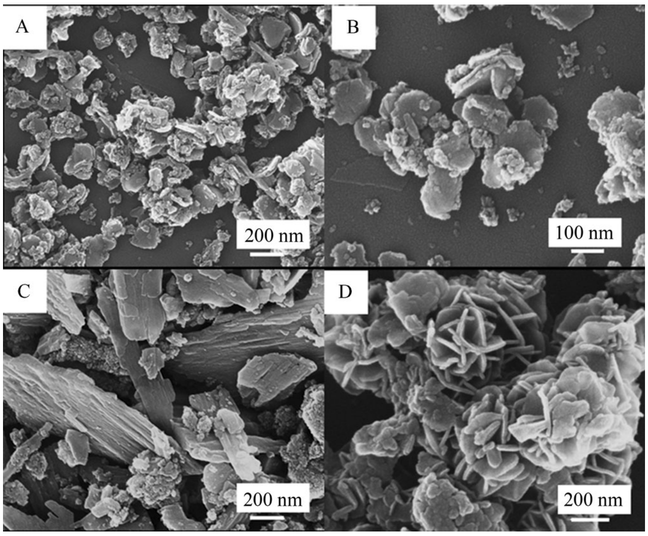

Figure 2. SEM images of NiTi–LDH at A) low magnification and B) high magnification. C) ZnTi–LDH and D) MgAlTi–LDH.

SEM images of the NiTi–LDH materials (Figure 2A and B) show that the particle sizes range between 100 and 200 nm. ZnTi–LDH exhibits sheetlike nanocrystals (Figure 2C), and the as-synthesized MgAlTi–LDH is composed of numerous nanoflakes (200–500 nm in diameter) that intercross with each other (Figure 2D). Figure S3A in the Supporting Information shows the diffuse reflectance UV/Vis spectra of the three Ti-containing LDH samples. An absorption band in the 200–400 nm region for these LDH materials was observed, which can be attributed to the ligand-to-metal charge transfer that involves the octahedral coordination of

Ti atoms in the brucite-like sheets.[16b] Moreover, the NiTi–LDH shows a broad absorption in the blue region (550–900 nm), which is due to the existence of Ni cations in the host layer. Moreover, UV/Vis diffuse reflectance spectra of the samples were also used to determine the bandgap (Figure S3B in the Supporting Information), from which bandgaps of approximately 2.41, 3.12, 3.52, and 3.40 eV were obtained for NiTi–LDH, ZnTi–LDH, MgAlTi–LDH, and Ti oxide, respectively. The narrow bandgap of NiTi– and ZnTi–LDH might facilitate their photocatalytic activity.

To further investigate the structural information of the Ti-containing LDHs, the materials were detected by high-resolution transmission electron microscopy (HRTEM). A typical TEM image (Figure 3a) reveals that the sample of NiTi–LDH displays platelike morphology with a lateral dimension of 100–200 nm; the lattice fringe (Figure 3b) indicates the single-crystalline nature of the NiTi–LDH material. The interplanar spacing is approximately 0.24 nm, which corresponds to the (012) plane of the NiTi–LDH phase. This value is in accordance with the in-plane structural parameter of the NiTi–LDH crystal determined from the XRD characterization ($d_{012} = 0.24$ nm). The energy-dispersive X-ray spectrometry (EDX) analysis of the NiTi–LDH (Figure 2c) shows the presence of Ni, Ti, and O with a Ni/Ti molar ratio of approximately 3.8, which nearly matches the nominal ratio (Ni/Ti = 4.0). ZnTi–LDH and MgAlTi–LDH also show high crystallinity tested by HRTEM, as shown in Figure S4 in the Supporting Information. Scanning transmission electron microscopy (STEM) was employed to gain further insight into the elemental distribution in the as-prepared NiTi–LDH sample. Figure 3d shows a HAADF micrograph of NiTi–LDH; Figure 3e and f display the elemental mapping of Ni and Ti, respectively, from which a uniform and homogeneous distribution of both Ni and Ti was observed with a discrimination of approximately 2 nm. In the case of the $K_2Ti_4O_9$ sample (Figure 3g), HRTEM observations reveal a whisker morphology with a length >1 μm and a diameter of approximately 500 nm. The interplanar spacing is 0.26 nm (Figure 3h), which corresponds to the (311) plane of $K_2Ti_4O_9$ (Figure S5 in the Supporting Information). Unlike the NiTi–LDH sample, serious aggregation of Ti was observed from the Ti mapping image (Figure 3i). On the basis of the results above, it can be concluded that Ti is located in a high dispersion in the LDH matrix, whereas it adopts an aggregation state in the $K_2Ti_4O_9$ sample. The dispersion state of TiO_6 imposes a key influence on its photocatalytic behavior, which will be discussed in the next section.

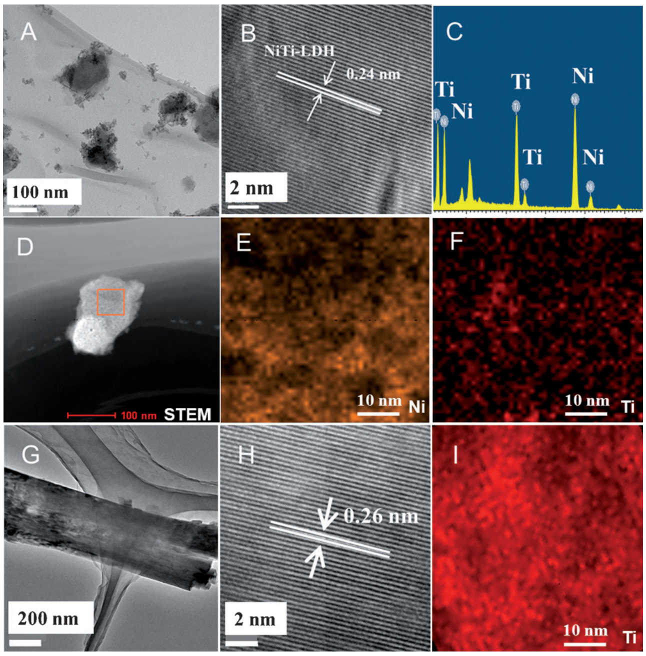

Figure 3. A) TEM image of NiTi–LDH with Ni^{2+}/Ti^{4+} molar ratio of 4:1; B) high-magnification TEM image of NiTi–LDH; C) the corresponding EDX spectrum of the NiTi–LDH; D) HAADF-STEM image of NiTi–LDH (the square diagram shows the mapping area of the sample). E) Elemental mapping images of Ni and F) Ti for the sample of NiTi–LDH; HRTEM images of $K_2Ti_4O_9$ at G) low magnification and F) high magnification. I) Elemental mapping image of Ti for $K_2Ti_4O_9$.

The detailed structure of Ti in the LDH matrix was carried out by XPS spectroscopy with $K_2Ti_4O_9$ as a comparison sample. As shown in Figure 4, the XPS spectrum of $K_2Ti_4O_9$ exhibits a Ti $2p_{3/2}$ peak at 457.8 eV on account of the O-Ti-O-Ti structure.[17] Upon dispersing TiO_6 units into the LDH matrix, the binding energy of Ti $2p_{3/2}$ shifted to 455.8 eV (NiTi–LDH) and 457.5 eV (ZnTi–LDH), respectively. It is known that the binding energy of a metal is determined by the positive potential that results from the specific arrangement of the ion core and electrons. The decrease in the binding energy of Ti $2p_{3/2}$ for the LDH materials is on account of a weaker bond situation by the introduction of dispersant (Ni or Zn) relative to the Ti^{IV}-O-Ti^{IV} bonding in

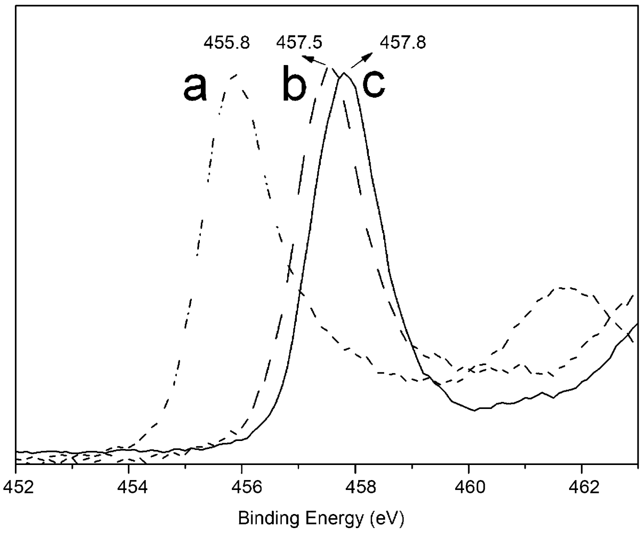

Figure 4. XPS spectra for Ti 2p3/2: a) NiTi–LDH, b) ZnTi–LDH, and c) $K_2Ti_4O_9$.

© 2012 Wiley-VCH Verlag GmbH & Co. KGaA, Weinheim

$K_2Ti_4O_9$.[11c] The results above indicate that the dispersion of TiO_6 units in the LDH matrix leads to the decrease in its positive potential with metal-to-metal charge-transfer transition, which would play a key role in determining the resulting catalytic performance.

Sorption analysis: The Ti-containing LDHs were analyzed by nitrogen-sorption measurements to shed light on the surface area and pore-size distribution properties. The N_2 adsorption–desorption isotherms of the obtained NiTi–LDH, ZnTi–LDH, and MgAlTi–LDH (Figure 5A) are type IV with H3-type hysteresis loop ($P/P_0 > 0.4$), which suggests the presence of mesopores. Furthermore, no limiting adsorption at higher P/P_0 was observed, thus indicating the existence of macropores.[18] Figure 5B shows that the modal pore diameter of the Ti-containing LDHs is in the range of 3–8 nm with a maximum at 3.8–4.8 nm. A large difference in the specific surface area for these LDH materials was found (Table 1): the NiTi–LDH shows the largest value (148.8 m^2g^{-1}), whereas the MgAlTi–LDH exhibits the lowest one (38.9 m^2g^{-1}), which might be attributed to the stacking of LDH nanoparticles (as shown in Figure 2D).

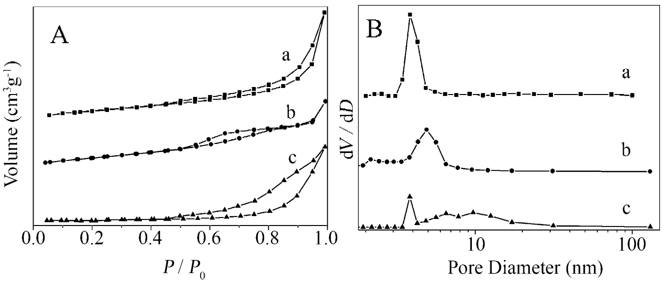

Figure 5. A) N_2-sorption isotherm and B) pore-size distribution of the Ti-containing LDHs: a) NiTi–LDH, b) ZnTi–LDH, and c) MgAlTi–LDH.

Table 1. BET surface area and mean pore diameter of the Ti-containing LDHs.

Sample	BET surface area [m^2g^{-1}]	Mean pore diameter [nm]
NiTi–LDH	148.8	3.8
ZnTi–LDH	128.5	4.8
MgAlTi–LDH	38.9	3.8

Photocatalytic performance of the LDH materials for splitting water into hydrogen: The photocatalytic properties of these LDH materials for water splitting into H_2 was evaluated under UV/Vis irradiation by using lactic acid as a sacrificial reagent and Pt as a cocatalyst. The sacrificial reagent provides electrons to consume the photogenerated holes, and Pt reduces the overpotential in the production of H_2 from water and suppresses the fast backward reaction (recombination of hydrogen and oxygen into water) as well.[19] Control experiments indicate that no appreciable hydrogen production was detected in the absence of either photocatalyst or irradiation, thereby suggesting that hydrogen can only be produced by photocatalytic reaction on catalysts. As shown in Figure 6, $K_2Ti_4O_9$ only generates a small amount of hydrogen (1.7 μmolh^{-1}), whereas the LDH materials evolve H_2 steadily from aqueous solution. The Ti-containing LDHs display a photocatalytic activity with the following sequence: ZnTi–LDH (31.4 μmolh^{-1}) > NiTi–LDH (15.3 μmolh^{-1}) > MgAlTi–LDH (4.9 μmolh^{-1}). The results above show that the Ti-containing LDHs exhibit much higher photocatalytic activity than that of the layered sample $K_2Ti_4O_9$. Abe et al. reported that the highly dispersed active metal can help to increase the photocatalytic active sites and promote the efficiency of electron–hole separation.[7] The largely enhanced photocatalytic performance of Ti-containing LDHs in this work can be attributed to the highly dispersive TiO_6 octahedra in the LDH matrix, which has been verified by STEM and XPS.

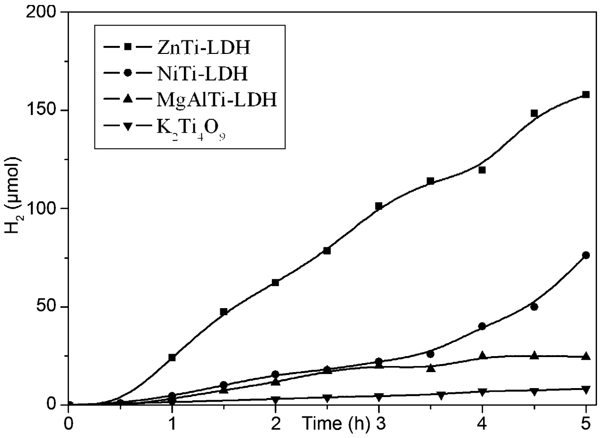

Figure 6. H_2 evolution from aqueous solution of lactic acid as sacrificial electron donor. Conditions: 100 mg of catalyst, 300 W Xe-lamp irradiation, 150 mL of degassed lactic acid solution (0.133 vol %).

A different molar ratio of M^{II}/Ti would influence the chemical and electric surroundings of the dispersed TiO_6 units as well as the resulting photocatalytic performance, and therefore the activity of NiTi–LDH as a function of molar ratio of Ni/Ti was studied. The XRD patterns of NiTi–LDH samples with various Ni/Ti ratios are shown in Figure S6 in the Supporting Information, the reflections of which can be indexed to an LDH phase for these samples. For the water-splitting reaction, NiTi–LDH with 4:1 displays the highest photocatalytic activity (15.3 μmolh^{-1}) relative to the 4.9, 2.7, and 2.0 μmolh^{-1} of the samples with Ni/Ti = 2:1, 3:1, and 5:1, respectively (Figure 7).

This might be attributed to the highest crystallinity of the LDH with Ni/Ti = 4:1, which results in superior dispersion of TiO_6 units. Moreover, XRD patterns of ZnTi–LDH with different Zn/Ti ratios are shown in Figure S7 in the Supporting Information, from which zinc hydroxide and TiO_2 impurities were observed for the samples of Zn/Ti = 3:1 and 4:1. The ZnTi–LDH with 2:1 displays the highest photocatalytic activity (31.4 μmolh^{-1}), relative to 14.0 and 12.5 μmolh^{-1} of the samples with Zn/Ti = 3:1 and 4:1, respectively (Figure 8).

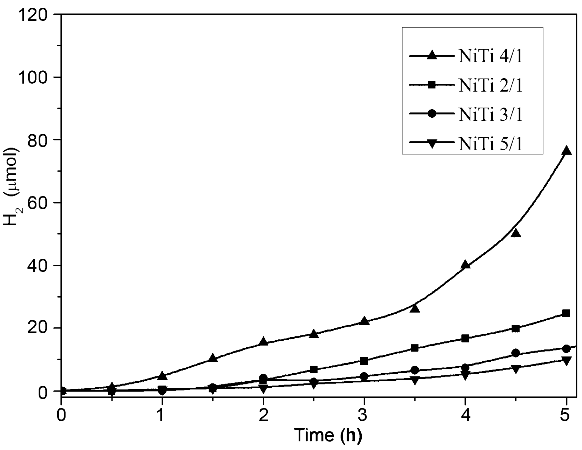

Figure 7. H_2 evolution in the presence of NiTi–LDHs with molar different ratios of Ni/Ti.

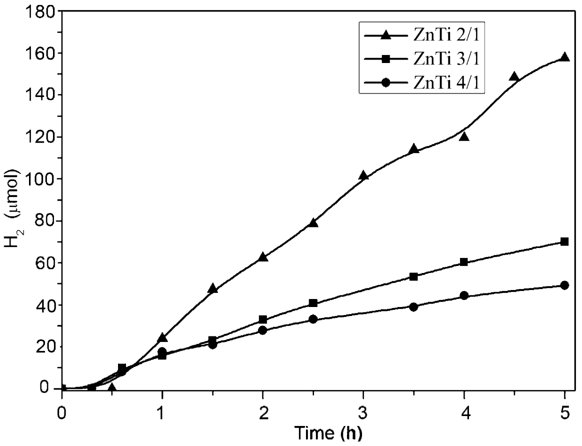

Figure 8. H_2 evolution in the presence of ZnTi–LDHs with different molar ratios of Zn/Ti.

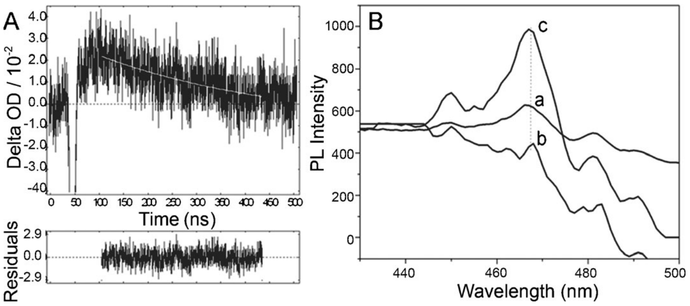

Figure 9. A) Transient absorption for the NiTi–LDH in H_2O (pumped at 266 nm and probed at 613 nm). NiTi–LDH exhibits exponential decays of 377.7 ns with χ^2 values of 0.77. B) Fluorescence spectra of a) NiTi–LDH, b) ZnTi–LDH, and c) $K_2Ti_4O_9$.

In addition, the long-term service performance of the NiTi–LDH (Ni/Ti = 4:1) and ZnTi–LDH (Zn/Ti = 2:1) was also tested. It maintained a constant photocatalytic activity ($\approx$15 and $\approx$30 μmol h^{-1}, respectively) over four consecutive cycles (Figure S8 in the Supporting Information). These results indicate that the Ti-containing LDHs can be used as promising photocatalysts for water splitting with high activity, long-term sustainability, and excellent recyclability.

To gain further insight into the photogenerated electron and hole activity in the LDH matrix, the electron–hole recombination kinetics of the NiTi–LDH with pure crystallinity was studied by transient-absorption (pump–probe) spectroscopic measurements. This absorption feature has been observed for various nanoparticles and is typically attributed to interband transitions of charge carriers trapped in mid-band states.[6a,20] The resulting absorption decay of the electron population for NiTi–LDH upon direct excitation at 266 nm is shown in Figure 9A. A single exponential fit to this spectrum yields a time constant of 377.7 ns; whereas 132.8 ns was obtained for the TiO_2 nanocrystals (Degussa P25) under the same conditions (Figure S9 in the Supporting Information). The larger time constant for the NiTi–LDH indicates slower electron–hole recombination kinetics, which possibly results from the defects in the bulk or on the surface of the NiTi–LDH sample that serve as trapping sites for photogenerated electrons.[21] This will be further discussed in the following section. The photoluminescence (PL) behavior is related to the transfer of the photoinduced electrons and holes, which can reflect the separation and recombination of photoinduced charge carriers.[22] In this study, the PL emission spectra of the Ti-containing LDHs and $K_2Ti_4O_9$ sample were examined in the 430–500 nm wavelength range (Figure 9B). It can be seen that $K_2Ti_4O_9$ shows a strong emission peak at approximately 466 nm ($\lambda_{ex} = 366$ nm), whereas the observed PL intensities of the NiTi–LDH and ZnTi–LDH are much weaker than that of $K_2Ti_4O_9$ with the sequence order: NiTi < ZnTi < $K_2Ti_4O_9$. This confirms the lower efficiency of electron–hole recombination upon dispersing TiO_6 units within an LDH matrix. The results of both transient-absorption and PL spectra demonstrate that a lower electron–hole recombination process occurs in the LDH materials relative to $K_2Ti_4O_9$, thus accounting for their significantly improved photocatlytic activity in water splitting.

It is well known that the majority of photogenerated electron–hole recombination occurs in bulk defects or on surface defects, thereby resulting in a quite moderate photoactivation efficiency.[23] Surface defects serve as charge-carrier traps as well as adsorption sites at which the charge transfer to adsorbed species can prevent electron–hole recombination, whereas bulk defects only act as charge-carrier traps where electrons and holes recombine.[24–26] Recently, Kong et al. reported that the increase in the ratio of surface defects to bulk defects for TiO_2 nanocrystals can significantly improve the separation efficiency of photogenerated electrons and holes and the resulting photocatalytic efficiency.[23] As a result, in this work, the properties of the defects were explored by positron annihilation, which is a well-established technique for the study of defects in materials. Table 2 lists three positron lifetime components (τ_1, τ_2, and τ_3) as well as their relative intensities (I_1, I_2, and I_3) for NiTi–

Table 2. Positron lifetimes and relative intensities of NiTi–LDH, $K_2Ti_4O_9$, and $Ni(OH)_2$.

Sample	τ_1 [ps]	τ_2 [ps]	τ_3 [ns]	I_1 [%]	I_2 [%]	I_3 [%]	I_2/I_1
LDH	183.6	367.1	1.888	36.97	60.36	2.67	1.63
$K_2Ti_4O_9$	206.9	338.7	2.011	45.80	52.80	1.40	1.15
$Ni(OH)_2$	231.6	365.5	2.206	53.20	45.30	1.50	0.85

LDH, $K_2Ti_4O_9$, and $Ni(OH)_2$, respectively. The longest component (τ_3) for all these samples is probably due to the annihilation of orthopositronium atoms formed in the large pores that are present in the material.[24] The shortest one (τ_1) is generally attributed to the free annihilation of positrons in the crystal such as monovacancies or oxygen vacancies,[23,25] which mainly exist in the bulk section of materials. The moderate τ_2 arises from positrons trapped by large size defects such as oxygen-vacancy clusters (i.e., dimers, trimers, or larger),[26] which have a tendency to be located on the surface or subsurface of the samples.[23,27] In addition to the lifetime of the positron, the relative intensity (I) provides information on the relative concentration of different defects.[23] The ratio of I_2/I_1 for NiTi–LDH is 1.63, much larger than that of $K_2Ti_4O_9$ and $Ni(OH)_2$ (1.15 and 0.85, respectively), which indicates the predominance of large-sized surface defects (I_2) for the NiTi–LDH material over $K_2Ti_4O_9$ and $Ni(OH)_2$. The results show that a high degree of surface defects can be obtained by distributing TiO_6 units into an LDH matrix; these serve as trapping sites for electrons and thus improve electron–hole separation efficiency. This is in accordance with the results of transient-absorption and PL spectroscopy.

EXAFS measurements were also carried out so as to study the local environment of the atoms in the layered materials. Figure S10 in the Supporting Information shows the Ni K-edge EXAFS Fourier transform spectra for NiTi–LDH and layered α-$Ni(OH)_2$. P1, P3, and P4 correspond to the first three oxygen shells, whereas P2 and P5–P8 mainly originate from the metallic neighbors at a, $\sqrt{3}a$, $2a$, $\sqrt{7}a$, and $3a$ (a is the cation–cation distance) from the absorbing atom, respectively.[28] As shown in Figure S10 in the Supporting Information, the first shell comprises oxygen atoms in the LDH or $Ni(OH)_2$ that possess a similar octahedral coordination.[28b] The results show that $Ni(OH)_2$ displays a coordination number of 6.6 and an Ni–O distance of 2.03 Å (Table S1 in the Supporting Information). However, after dispersing TiO_6 into the layered $Ni(OH)_2$, a decrease in coordination number of Ni (6.1) as well as a slight increase in the Ni–O distance (2.04 Å) were obtained. This indicates the increase of defects in the sample of NiTi–LDH. Therefore, the results of a refined coordination number in the shell (P1, P2) of Ni-O-Ni and Ni-O-Ti are in agreement with the results of positron annihilation.

In addition, the spin-trapping electron spin resonance (ESR) technique was employed to investigate the presence of active radicals (the electron and hole) formed on the surface of Ti-containing materials. As shown in Figure 10A, six characteristic peaks of DMPO–$O_2^{\bullet -}$ (DMPO = 5,5-dimethyl-1-pyrroline-*N*-oxide) were observed in methanol, with the intensity order NiTi–LDH > $K_2Ti_4O_9$. No signals could be detected without irradiation. Since $O_2^{\bullet -}$ results from the reaction of e_{cb}^- (cb = conduction-band electron) with surface-absorbed O_2,[29] the result indicates that the electron intensity on the surface of NiTi–LDH is larger than that of $K_2Ti_4O_9$. The same conclusion was obtained from Figure 10B, from which four characteristic peaks of DMPO–$^{\bullet}OH$ that originated from the reaction of h_{vb}^+ (vb = valence band) with the OH group can be clearly observed with the intensity order NiTi–LDH > $K_2Ti_4O_9$. The stronger intensity of photogenerated e_{cb}^- as well as h_{vb}^+ is in accordance with the results of transient absorption, PL behavior, and positron annihilation mentioned above, which accounts for the largely enhanced activity of Ti-containing LDH materials toward water splitting.

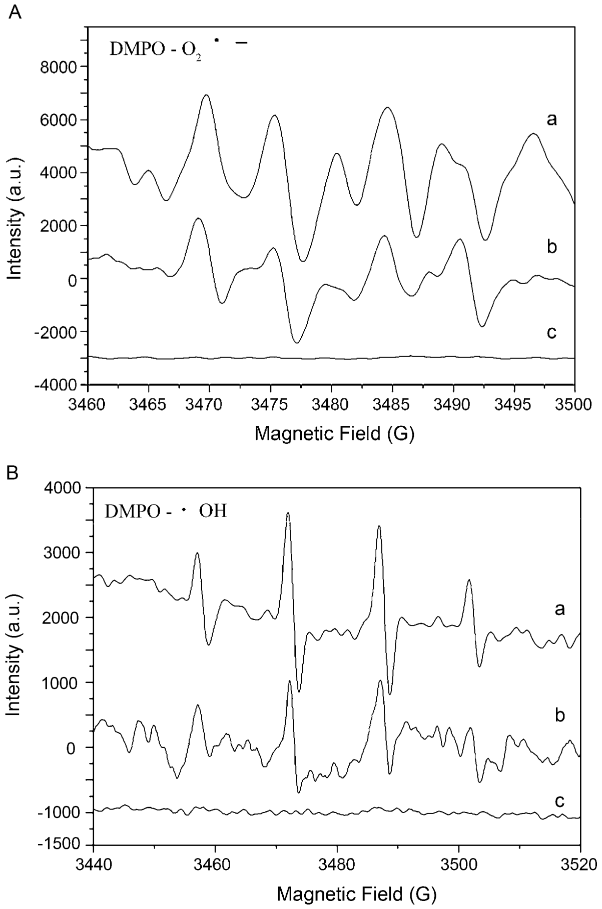

Figure 10. DMPO spin-trapping ESR spectra recorded for A) DMPO–$O_2^{\bullet -}$ in methanol dispersion and B) DMPO–$^{\bullet}OH$ in aqueous dispersion: a) NiTi–LDH, b) $K_2Ti_4O_9$–LDH, c) blank. Conditions: [DMPO] = 0.10 M, m_{cat} = 2 mg, $V_{solvent}$ = 0.5 mL, Xe lamp, ambient temperature.

The surface atomic configurations of TiO_6 units in the LDH and $K_2Ti_4O_6$: To understand the surroundings of the TiO_6 octahedra, the views of the surface atomic configurations for the NiTi–LDH and $K_2Ti_4O_9$ are shown in Figure 11. Figure 11a shows the LDH structure that is based on brucite-

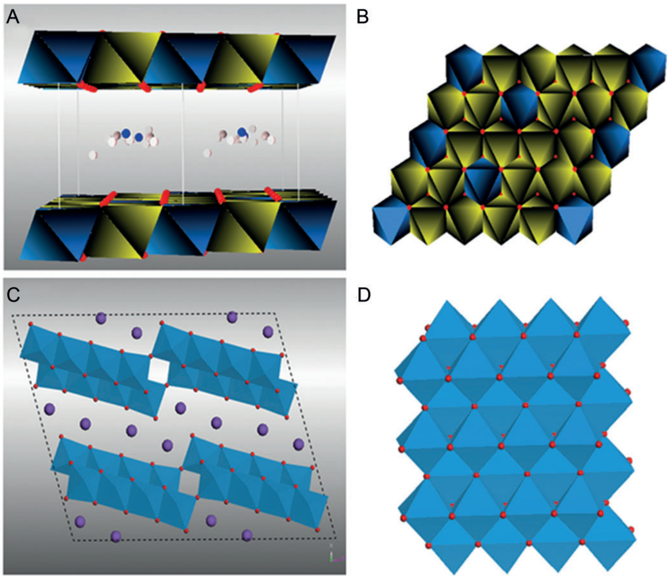

Figure 11. A) A polyhedral representation of the LDH structure showing the metal hydroxide octahedra stacking along the crystallographic *c* axis. Water and anions are present in the interlayer region. B) Vertical view of the surface atomic configurations for the LDH layer. Dark blue: Ti; yellow: Ni. C) Crystal structure of $K_2Ti_4O_9$. D) Vertical view of the surface atomic configurations for the TiO_6 octahedra in $K_2Ti_4O_9$.

like ($Mg(OH)_2$) layers of edge-sharing MO_6 octahedra; isomorphous substitution of part of the divalent M^{II} cations (yellow color) by Ti^{IV} cations (blue) generates positively charged sheets with charge-balancing anions in the interlayer gallery, and the hydroxide layers stack along the crystallographic *c* axis. The vertical view of the primitive cell for the (001) facet of LDH after geometry optimization is presented in Figure 11b, in which the Ni^{II} and Ti cations are orderly distributed in a honeycomb arrangement. Figure 11c shows the crystal structure of $K_2Ti_4O_9$, which consists of edge- and corner-shared TiO_6 octahedra that completely occupy the layer (Figure 11d). The results of HAADF-STEM mapping (Figure 3e and f) also demonstrate the high dispersion of Ti in the LDH matrix and the serious aggregation of Ti in $K_2Ti_4O_9$. Both the LDH and $K_2Ti_4O_9$ provide oxo bridges and multicoordinated oxygen atoms, which are common structures for the evolution of H_2 in photocatalytic water reduction.[7,30] The ordered dispersion of TiO_6 units affects the separation efficiency of the photogenerated electrons and holes, which plays a key role in determining the photocatalytic activity.

For the purpose of understanding the electronic structure of the Ti-containing materials and the resulting photocatalytic behavior, the band structure, the densities of states (DOS), as well as the partial densities of states (PDOS) for the ideal model of NiTi–LDH and $K_2Ti_4O_9$ were investigated respectively by density functional theory (DFT) calculations. As shown in Figure S11 in the Supporting Information, it was found that the valence-band (VB) maximum and conduction-band (CB) minimum of NiTi–LDH and $K_2Ti_4O_9$ are located at the same *Z* point = (0, 0, 1/2) of the brillouin zone, which indicates that both of them are direct semiconductors. The direct energy gap is approximately 2.1 eV for NiTi–LDH, much lower than that of $K_2Ti_4O_9$ (3.2 eV), which accounts for its high photocatalytic activity and agrees well with the experimental test results. Figure 12a shows the DOS and PDOS of the NiTi–LDH, from which it was found the VB top is primarily constructed by the occupied Ni 3d orbitals, whereas the CB bottom is mainly dominated by the unoccupied Ti 3d orbitals. The bandgap transitions from the VB top (HOMO) to the CB bottom (LUMO) mainly occur from the occupied Ni 3d orbitals to unoccupied Ti 3d orbitals. Additionally, a contribution from the O 2p orbitals in the LDH layers was also observed for both the HOMO and LUMO,[31] thus indicating a mixture of the O 2p, Ni 3d, and Ti 3d orbitals. It is noteworthy that Ni

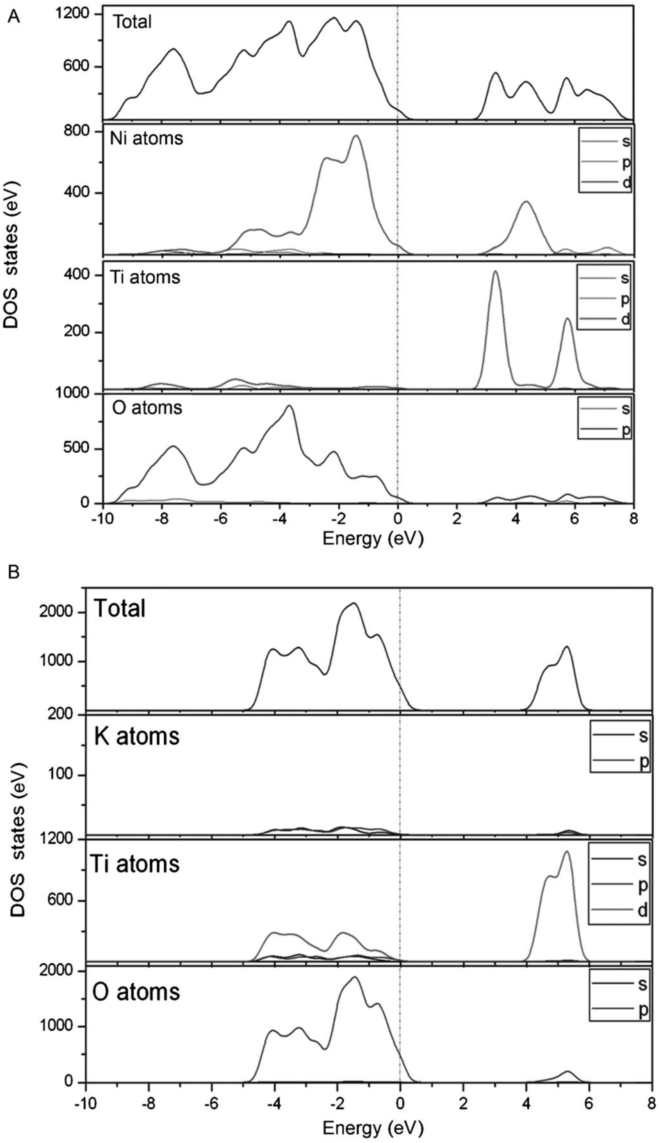

Figure 12. The total and partial density of states: A) NiTi–LDH and B) $K_2Ti_4O_9$.

© 2012 Wiley-VCH Verlag GmbH & Co. KGaA, Weinheim

3d orbitals also make contribution to LUMO, thereby demonstrating the covalent interaction between Ni and Ti atoms. In the case of $K_2Ti_4O_9$ (Figure 12b), the O 2p orbitals contribute strongly to the VB top. Clear components of Ti were also found for the bands in the energy region from −5 to 0 eV, thus indicating the covalent interaction between Ti and O. The O 2p and Ti 3d make a significant contribution to the VB top of $K_2Ti_4O_9$,[6b] whereas there was no contribution between Ti and O. The O 2p and Ti 3d make a significant contribution to the VB top of $K_2Ti_4O_9$,[6b] whereas no contribution from K 2p orbitals is observed. The above results indicate that the TiO_6 octahedron itself in $K_2Ti_4O_9$ plays a key role in its photocatalytic activity. In the case of NiTi–LDH, however, the TiO_6 modified by the covalent interaction with NiO_6 plays a crucial role in the water-splitting behavior. It is proposed that the local coordination environment of TiO_6 units (metal–oxygen–metal bond) in NiTi–, ZnTi–, and MgAlTi–LDH would have a significant influence on the electronic structure and bandgap of the TiO_6 units as well as the resulting photocatalytic behavior.

Conclusion

MTi–LDHs (M = Ni, Zn, MgAl) were synthesized by the coprecipitation method. They display remarkable photocatalytic performance for water splitting into hydrogen. The Ti-containing LDH shows a photocatalytic H_2-production rate of $31.4\ \mu\text{mol}\,\text{h}^{-}$ with 0.133 vol % lactic acid as sacrificial electron donor, 18 times higher than that of $K_2Ti_4O_9$. Furthermore, its stability and recyclability in water splitting were also demonstrated. The structural and morphological studies reveal a high dispersion of TiO_6 octahedra in Ti–LDH, whereas there is serious aggregation in $K_2Ti_4O_9$. Both transient-absorption and PL spectra demonstrate that a lower electron–hole recombination process occurs in the LDH materials than in $K_2Ti_4O_9$ as a result of the abundant surface defects that serve as trapping sites for photogenerated electrons. DFT calculation results indicate that the photocatalytic activity of NiTi–LDH originates from the dispersed TiO_6 octahedra, the electronic structure of which is modified by the covalent interaction between TiO_6 and NiO_6. By virtue of the intrinsic dispersion of MO_6 units, it is expected that the synthetic strategy in this work can be extended to the preparation of other oxide or hydroxide catalysts with enhanced performance, and therefore that might have potential applications in photocatalysis and energy conversion.

Acknowledgements

This project was supported by the 973 Program (grant no. 2011CBA00504), the National Natural Science Foundation of China, the 111 Project (grant no. B07004), and the Collaboration Project from the Beijing Education Committee. The authors are grateful to Dr. Haimei Liu from Beijing University of Chemical Technology and Prof. Dermot O'Hare from University of Oxford for the helpful discussions.

---

[1] a) H. Yan, J. Yang, G. Ma, G. Wu, X. Zong, Z. Lei, J. Shi, C. Li, *J. Catal.* **2009**, *266*, 165; b) W. J. Youngblood, S. H. Lee, K. Maeda, T. E. Mallouk, *Acc. Chem. Res.* **2009**, *42*, 1966; c) F. E. Osterloh, *Chem. Mater.* **2008**, *20*, 35; d) X. Zong, C. Sun, Z. Chen, A. Mukherji, H. Wu, J. Zou, S. C. Smith, G. Q. Lu, L. Wang, *Chem. Commun.* **2011**, *47*, 6293; e) X. Zong, H. Yan, G. Wu, G. Ma, F. Wen, L. Wang, C. Li, *J. Am. Chem. Soc.* **2008**, *130*, 7176; f) M. Kitano, M. Hara, *J. Mater. Chem.* **2010**, *20*, 627; g) S. C. Roy, O. K. Varghese, M. Paulose, C. A. Grimes, *ACS Nano* **2010**, *4*, 1259; h) C.-J. Liu, U. Burghaus, F. Besenbacher, Z. L. Wang, *ACS Nano* **2010**, *4*, 5517; i) K. Maeda, K. Teramura, D. Lu, T. Takata, N. Saito, Y. Inoue, K. Domen, *Nature* **2006**, *440*, 295; j) Z. Zou, J. Ye, K. Sayama, H. Arakawa, *Nature* **2001**, *414*, 625.

[2] a) T. Matoba, K. Maeda, K. Domen, *Chem. Eur. J.* **2011**, *17*, 14731; b) N. Ahmed, Y. Shibata, T. Taniguchi, Y. Izumi, *J. Catal.* **2011**, *279*, 123; c) S. C. Yan, S. X. Ouyang, J. Gao, M. Yang, J. Y. Feng, X. X. Fan, L. J. Wan, Z. S. Li, J. H. Ye, Y. Zhou, Z. G. Zou, *Angew. Chem.* **2010**, *122*, 6544; *Angew. Chem. Int. Ed.* **2010**, *49*, 6400; d) X. Wang, K. Maeda, A. Thomas, K. Takanabe, G. Xin, J. M. Carlsson, K. Domen, M. Antonietti, *Nat. Mater.* **2009**, *8*, 76; e) X. Chen, L. Liu, P. Y. Yu, S. S. Mao, *Science* **2011**, *331*, 746; f) X. Yang, C. Salzmann, H. Shi, H. Wang, M. L. H. Green, T. Xiao, *J. Phys. Chem. A* **2008**, *112*, 10784.

[3] a) A. Kudo, Y. Miseki, *Chem. Soc. Rev.* **2009**, *38*, 253; b) Y. Inoue, *Energy Environ. Sci.* **2009**, *2*, 364; c) X. Chen, S. S. Mao, *Chem. Rev.* **2007**, *107*, 2891; d) K. Maeda, K. Domen, *J. Phys. Chem. C* **2007**, *111*, 7851; e) J. Sato, H. Kobayashi, K. Ikarashi, N. Saito, H. Nishiyama, Y. Inoue, *J. Phys. Chem. B* **2004**, *108*, 4369.

[4] a) A. Kudo, K. Sayama, A. Tanaka, K. Asakura, K. Domen, K. Maruya, T. Onishi, *J. Catal.* **1989**, *120*, 337; b) K. Sayama, A. Tanaka, K. Domen, K. Maruya, T. Onishi, *J. Phys. Chem.* **1991**, *95*, 1345; c) A. Kudo, H. Kato, *Chem. Lett.* **1997**, *26*, 867; d) F. Geng, R. Ma, T. Sasaki, *Acc. Chem. Res.* **2010**, *43*, 1177; e) C. Gomes Silva, R. Juarez, T. Marino, R. Molinari, H. Garcıa, *J. Am. Chem. Soc.* **2011**, *133*, 595.

[5] a) J. S. Jang, H. G. Kim, V. R. Reddy, S. W. Bae, S. M. Ji, J. S. Lee, *J. Catal.* **2005**, *231*, 213; b) G. Liu, L. Wang, C. Sun, X. Yan, X. Wang, Z. Chen, S. C. Smith, H. M. Cheng, G. Q. Lu, *Chem. Mater.* **2009**, *21*, 1266; c) H. Hata, Y. Kobayashi, V. Bojan, W. J. Youngblood, T. E. Mallouk, *Nano Lett.* **2008**, *8*, 794; d) Y. Kobayashi, M. Tian, M. Eguchi, T. E. Mallouk, *J. Am. Chem. Soc.* **2009**, *131*, 9849.

[6] a) M. R. Allen, A. Thibert, E. M. Sabio, N. D. Browning, D. S. Larsen, F. E. Osterloh, *Chem. Mater.* **2010**, *22*, 1220; b) T. Guo, L. Wang, D. G. Evans, W. Yang, *J. Phys. Chem. C* **2010**, *114*, 4765; c) X. Sun, X. Chen, Y. Li, *Inorg. Chem.* **2002**, *41*, 4996; d) Q. Wang, Z. Guo, J. S. Chung, *Chem. Commun.* **2009**, 5284; e) Q. Wang, S. Y. Park, L. Duan, J. S. Chung, *Appl. Catal. B* **2008**, *85*, 10.

[7] a) R. Abe, M. Higashi, K. Sayama, Y. Abe, H. Sugihara, *J. Phys. Chem. B* **2006**, *110*, 2219; b) Y. Shimodaira, H. Kato, H. Kobayashi, A. Kudo, *J. Phys. Chem. B* **2006**, *110*, 17790; c) H. Hagiwara, T. Inoue, K. Kaneko, T. Ishihara, *Chem. Eur. J.* **2009**, *15*, 12862; d) M. Anpo, H. Yamashita, K. Ikeue, Y. Fujii, S. G. Zhang, Y. Ichihashi, D. R. Park, Y. Suzuki, K. Koyano, T. Tatsumi, *Catal. Today* **1998**, *44*, 327; e) G. Blasse, *Struct. Bonding (Berlin)* **1991**, *76*, 153.

[8] a) B. Qiao, A. Wang, X. Yang, L. F. Allard, Z. Jiang, Y. Cui, J. Liu, J. Li, T. Zhang, *Nat. Chem.* **2011**, *3*, 634; b) A. A. Herzing, C. J. Kiely, A. F. Carley, P. Landon, G. J. Hutchings, *Science* **2008**, *321*, 1331; c) X. Sun, J. Lin, *J. Phys. Chem. C* **2009**, *113*, 4970; d) D. Brühwiler, H. Frei, *J. Phys. Chem. B* **2003**, *107*, 8547; e) W. Lin, H. Frei, *J. Am. Chem. Soc.* **2005**, *127*, 1610; f) H. Han, H. Frei, *J. Phys. Chem. C* **2008**, *112*, 16156; g) R. Nakamura, A. Okamoto, H. Osawa, H. Irie, K. Hashimoto, *J. Am. Chem. Soc.* **2007**, *129*, 9596.

[9] a) J. A. Rodriguez, S. Ma, P. Liu, J. Hrbek, J. Evans, M. Pérez, *Science* **2007**, *318*, 1757; b) F. Raimondi, G. G. Scherer, R. Kotz, A. Wokaun, *Angew. Chem.* **2005**, *117*, 2228; *Angew. Chem. Int. Ed.* **2005**, *44*, 2190; c) S. H. Joo, J. Y. Park, C.-K. Tsung, Y. Yamada, P. Yang, G. A. Somorjai, *Nat. Mater.* **2009**, *8*, 126; d) M. Q. Zhao, Q. Zhang, J. Q. Huang, F. Wei, *Adv. Funct. Mater.* **2012**, *22*, 675; e) R.

© 2012 Wiley-VCH Verlag GmbH & Co. KGaA, Weinheim

Ma, T. Sasaki, *Adv. Mater.* **2010**, *22*, 5082; f) D. Wu, F. Zhang, P. Liu, X. Feng, *Chem. Eur. J.* **2011**, *17*, 10804.

[10] a) P. J. Sideris, U. G. Nislsen, Z. Gan, C. P. Grey, *Science* **2008**, *321*, 113; b) Q. Wang, D. O'Hare, *Chem. Rev.* **2012**, *112*, 4124; c) D. G. Evans, X. Duan, *Chem. Commun.* **2006**, 485; d) L. Li, R. Z. Ma, Y. Ebina, K. Fukuda, K. Takada, T. Sasaki, *J. Am. Chem. Soc.* **2007**, *129*, 8000; e) M. Q. Zhao, Q. Zhang, W. Zhang, J. Q. Huang, Y. Zhang, D. S. Su, F. Wei, *J. Am. Chem. Soc.* **2010**, *132*, 14739; f) G. R. Williams, D. O'Hare, *J. Mater. Chem.* **2006**, *16*, 3065; g) D. Yan, J. Lu, M. Wei, D. G. Evans, X. Duan, *J. Mater. Chem.* **2011**, *21*, 13128; h) Y. Zhao, M. Wei, J. Lu, Z. L. Wang, X. Duan, *ACS Nano* **2009**, *3*, 4009; i) Y. Zhao, S. He, M. Wei, D. G. Evans, X. Duan, *Chem. Commun.* **2010**, *46*, 3031; j) G. Hu, D. O'Hare, *J. Am. Chem. Soc.* **2005**, *127*, 17808; k) C. J. Wang, Y. A. Wu, R. M. J. Jacobs, J. H. Warner, G. R. Williams, D. O'Hare, *Chem. Mater.* **2011**, *23*, 171.

[11] a) C. G. Silva, Y. Bouizi, V. Fornés, H. García, *J. Am. Chem. Soc.* **2009**, *131*, 13833; b) J. L. Gunjakar, T. W. Kim, H. N. Kim, I. Y. Kim, S. J. Hwang, *J. Am. Chem. Soc.* **2011**, *133*, 14998; c) Y. Lee, J. H. Choi, H. J. Jeon, K. M. Choi, J. W. Lee, J. K. Kang, *Energy Environ. Sci.* **2011**, *4*, 914; d) Y. Zhao, S. Zhang, B. Li, H. Yan, S. He, L. Tian, W. Shi, J. Ma, M. Wei, D. G. Evans, X. Duan, *Chem. Eur. J.* **2011**, *17*, 13175.

[12] X. Shu, Z. An, L. Wang, J. He, *Chem. Commun.* **2009**, 5901.

[13] M. Shao, J. Han, M. Wei, D. G. Evans, X. Duan, *Chem. Eng. J.* **2011**, *168*, 519.

[14] N. Das, A. Samal, *Microporous Mesoporous Mater.* **2004**, *72*, 219.

[15] M. He, X. Feng, X. H. Lu, X. Y. Ji, C. Liu, N. Z. Bao, J. W. Xie, *J. Mater. Sci.* **2004**, *39*, 3745.

[16] a) W. H. Zhang, X. D. Guo, J. He, Z. Y. Qian, *J. Eur. Ceram. Soc.* **2008**, *28*, 1623; b) E. M. Seftel, E. Popovici, M. Mertens, G. V. Tendeloo, P. Cool, E. F. Vansant, *Microporous Mesoporous Mater.* **2008**, *111*, 12; c) B. Mavis, M. Akinc, *Chem. Mater.* **2006**, *18*, 5317.

[17] J. Dupin, D. Gonbeau, P. Vinatier, A. Levasseur, *Phys. Chem. Chem. Phys.* **2000**, *2*, 1319.

[18] L. Zhou, W. Z. Wang, H. L. Xu, S. M. Sun, M. Shang, *Chem. Eur. J.* **2009**, *15*, 1776.

[19] Q. Li, B. Guo, J. Yu, J. Ran, B. Zhang, H. Yan, J. R. Gong, *J. Am. Chem. Soc.* **2011**, *133*, 10878.

[20] a) E. C. Carroll, O. C. Compton, D. Madsen, F. E. Osterloh, D. S. Larsen, *J. Phys. Chem. C* **2008**, *112*, 2394; b) Y. Tamaki, A. Furube, M. Murai, K. Hara, R. Katoh, M. Tachiya, *Phys. Chem. Chem. Phys.* **2007**, *9*, 1453.

[21] A. Furube, T. Shiozawa, A. Ishikawa, A. Wada, K. Domen, C. Hirose, *J. Phys. Chem. B* **2002**, *106*, 3065.

[22] F. B. Li, X. Z. Li, *Appl Catal. A* **2002**, *228*, 15.

[23] M. Kong, Y. Li, X. Chen, T. Tian, P. Fang, F. Zheng, X. Zhao, *J. Am. Chem. Soc.* **2011**, *133*, 16414.

[24] S. Chakraverty, S. Mitra, K. Mandal, P. M. G. Nambissan, S. Chattopadhyay, *Phys. Rev. B* **2005**, *71*, 024115.

[25] D. Sanyal, D. Banerjee, U. De, *Phys. Rev. B* **1998**, *58*, 15226.

[26] X. W. Liu, K. B. Zhou, L. Wang, B. Y. Wang, Y. D. Li, *J. Am. Chem. Soc.* **2009**, *131*, 3140.

[27] W. Sun, Y. Z. Li, W. Q. Shi, X. J. Zhao, P. F. Fang, *J. Mater. Chem.* **2011**, *21*, 9263.

[28] a) H. Roussel, V. Briois, E. Elkaim, A. De Roy, J. P. Besse, *J. Phys. Chem. B* **2000**, *104*, 5915; b) S. Gago, M. Pillinger, A. A. Valente, T. M. Santos, J. Rocha, I. S. Goncüalves, *Inorg. Chem.* **2004**, *43*, 5422.

[29] Z. Li, Z. Xie, Y. Zhang, L. Wu, X. Wang, X. Fu, *J. Phys. Chem. C* **2007**, *111*, 18348.

[30] D. Wang, H. Jiang, X. Zong, Q. Xu, Y. Ma, G. Li, C. Li, *Chem. Eur. J.* **2011**, *17*, 1275.

[31] D. Yan, J. Lu, M. Wei, J. Han, J. Ma, F. Li, D. G. Evans, X. Duan, *Angew. Chem.* **2009**, *121*, 3119; *Angew. Chem. Int. Ed.* **2009**, *48*, 3073.

Received: March 29, 2012
Published online: August 27, 2012

© 2012 Wiley-VCH Verlag GmbH & Co. KGaA, Weinheim